Monte Carlo Network Simulation of Horizontal, Upflow and Downflow Depth Filtration

V. N. Burganos, C. A. Paraskeva, and A. C. Payatakes
Inst. of Chemical Engineering and High Temperature Chemical Processes and Dept. of Chemical Engineering
University of Patras, GR 26500 Patras, Greece

A test particle trajectory approach is developed for the simulation of deep bed filtration. A 3-D network of constricted pores represents the pore space of granular filters, network-scale trajectories of a large number of non-Brownian test particles are computed, and filter coefficient predictions are obtained for horizontal, down- and upflow filtration operation. This simulator yields numerical results that agree excellently with our earlier predictions by the pore-scale trajectory-based population balance method. The new approach, however, circumvents the cumbersome step of calculating the impacted fraction in each unit cell, which the earlier method required, by providing direct statistical estimates of the local and overall deposition rates for continuous and discrete pore-size distributions. For large superficial velocities ($v_s > \sim 1$ mm/s) and distributed pore size, downflow filters are more efficient than horizontal flow filters, whereas for small velocities ($v_s < \sim 0.5$ mm/s) the opposite is observed. Horizontal flow operation is also favored by uniform packing for almost any value of the external pressure gradient. Upflow operation is the least efficient for the packings considered here over a broad range of superficial velocity and particle-size values. Observed differences among the three filtration types are maximal for uniform packings and decrease considerably with increasing packing heterogeneity.

Introduction

Deep bed filtration (DBF) is a well-known fluid-solid separation process and has been the subject of numerous experimental and theoretical investigations. Depth filters are used extensively in water and sewage tertiary treatment processes and, when combined with coagulation, are capable of yielding filtrates of exceptional clarity (Ives, 1990; Tien, 1989). Recently, Wegelin et al. (1987, 1991) reported an increasing use of depth filters in horizontal, downflow, and upflow operation for rural water pretreatment in developing countries. Such roughing filters are usually gravel packed and consist of several compartments with coarse (~20 mm in diameter) to progressively finer (to ~5 mm) particles (see also Ahsan et al., 1993). Their role is to reduce the solid matter concentration of surface water prior to the main filtration (usually slow sand filtration) and microbiological water quality improvement stages.

Design and optimization of application-tailored depth filters and filtration processes rely heavily on adequate understanding and description of the particle transport and deposition phenomena, and of the role of several important parameters including the filter microstructure, the flow mode and conditions, the particle-grain physicochemical and hydrodynamic interactions, and the stability of the flowing suspension. It has recently been recognized that the monitoring of particle motion through the packed bed provides a powerful means for the elucidation of the basic transport and capture mechanisms that support the aforementioned phenomena. Moreover, when "particle trajectory" based simulators and models are applied to pore or grain models of the filter structure, they can make quantitative predictions of the local and overall filtration rates. They offer the possibility of following the temporal evolution of the pore space and deposit morphology, as well as the concomitant change of filtration efficiency and reduction of permeability.

Several attempts to perform particle trajectory calculations in pore or grain models have appeared in the literature. They can be divided, roughly, into single and multiple collector

Correspondence concerning this article should be addressed to A. C. Payatakes.

approaches. The former include single sphere models (Spielman and Goren, 1970; Yao et al., 1971; Spielman and Cukor, 1973; Rajagopalan and Tien, 1977; Vaidyanathan and Tien, 1988), capillary models (Payatakes et al., 1974a; Hung and Tien, 1976), and sphere-in-cell models (Vaidyanathan and Tien, 1988; FitzPatrick and Spielman, 1973; Spielman and FitzPatrick, 1973; Rajagopalan and Tien, 1976; Mackie et al., 1987). The first attempt to account for the combined action of multiple collectors led to the unit bed element (UBE) model that considered pores of converging-diverging geometry and variable size (Payatakes et al., 1973, 1974b, 1977; Tien and Payatakes, 1979; Pendse and Tien, 1982; Tien, 1989). Although pioneering in that respect, UBE-based models consider axisymmetric pores in the average flow direction only and, consequently, overlook the 3-D character of the particulate transport through the filter. The UBE concept was recently employed by Soo and Radke (1986) in their study of flow of dilute stable emulsions through unconsolidated porous media. Based on the UBE structure of the porous medium, these authors developed a filtration model that takes into account the flow-redistribution phenomenon caused by small pore plugging and concomitant shifting of flow pathways to progressively larger pores. Useful expressions for the drop retention and volume concentration profiles were developed in that work.

The contribution of lateral collecting surfaces to the overall deposition rate has been observed experimentally in several studies (for visualization studies of hydrosol filtration through glass micromodels, see Payatakes et al., 1981). Quantification of this contribution can potentially be provided in a straightforward manner by 3-D pore or grain models of depth filtration. Pore network models of DBF are discussed in the recent review article by Sahimi et al. (1990) and elsewhere (Rege and Fogler, 1988; Imdakm and Sahimi, 1991). Below, we discuss the most notable advancements.

Donaldson et al. (1977) presented an oversimplified model of particle transport through sandstones using a bundle of vertical capillaries with distributed pore sizes. Todd et al. (1984) simulated formation damage in oil reservoirs using a square network (constant pore size) and assuming diffusional motion for the solid particles (random walk). Houi and Lenormand (1986) used a square arrangement of identical spherical collectors and developed a procedure that could bias the particles towards the interior of the filter.

Imdakm and Sahimi (1987) simulated particle transport in a square network of cylindrical tubes and evaluated the permeability reduction as a function of time or injected pore volume. Particle and pore sizes were sampled from continuous size distributions. No actual particle trajectories within the pores were calculated in that work. The outcome of a particle entrance into a pore was solely determined by the relative size of the particle to that of the pore, a_p/R: if $a_p/R > 1$, pore clogging occurs, whereas, if $a_p/R < 1$, the particle is assumed to escape from the pore leaving the pore surface intact. Later, the same authors (Imdakm and Sahimi, 1991) included particle trajectory calculations in their simulations and provided estimates of the filter permeability and of the particle concentration as functions of time. Gradual reduction of the pore flow-conductances (caused by development of fine particle deposits) and reentrainment of captured material were taken into account in that work. However, the consideration of cylindrical pores only (which are known to be poor collectors and fail to represent efficiently the interstitial space of packed beds), and the restriction of particle trajectories to two dimensions within oblique pores raise some ambiguities about the reliability of the numerical results and of the conclusions presented there.

Sharma and Yortsos (1987a,b,c) considered transport of Brownian particles in pore networks and used a continuum population balance method for the calculation of the particle concentration profile. They assumed uniform coating on the pore surfaces and monitored the temporal evolution of the network permeability through the use of the effective medium approximation (EMA) (Kirkpatrick, 1973). Since the particle deposit buildup is considered in that work as nonporous, intensive pore clogging develops which causes drastic reduction of the network permeability. As the percolation threshold is approached, the EMA becomes progressively less accurate and may provide poor estimates of the filter permeability. Alternatively, one could use the standard network analysis for the calculation of the network permeability near the percolation threshold by solving numerically the mass balance equation at the pore intersection sites. This procedure was followed by Rege and Fogler (1987, 1988) who used a 2-D triangular network of cylindrical pores. In their earlier model (1987) particle deposition occurred through a straining mechanism ($a_p/R > 1$), whereas in their later work (1988), deposition within individual pores was controlled by an adjustable parameter.

A common shortcoming of all the aforementioned pore network models of depth filtration is the use of straight cylindrical tubes for the representation of the void space. However, not only does this assumption oversimplify the pore structure of unconsolidated media (such as packed beds), but it also leads to unacceptably low deposition rates and filter coefficients (Payatakes et al., 1974a; Tien and Payatakes, 1979). Pores with converging-diverging geometry offer a considerably better representation of the interstitial space of granular beds and, despite the increased computational effort that is required for the numerical solution of the flow equation in them, their use in filtration models is highly advantageous over that of cylindrical tubes.

Recently, we have addressed the most serious technical drawbacks of previous pore network models of depth filtration and presented a line of work that offers both a physically acceptable representation of the filter structure and a detailed particle transport simulator that accounts for pore segments that are not aligned with the average flow direction. Paraskeva et al. (1991) developed a 3-D particle trajectory analysis in pores of sinusoidal shape taking into account the hydrodynamic forces and torques, gravity, the London-van der Waals force, and the double ionic layer force. Extensive particle trajectory and impacted fraction calculations in pores with various inclinations showed that horizontal pores have a substantially increased collection efficiency compared to that of vertical pores for the same pressure drop. This crucial observation stimulated the development of a 3-D sinusoidal pore network simulator of depth filtration (Burganos et al., 1992). The pore sizes (mouth and constriction diameters) were sampled from prescribed size distributions, and the creeping flow conductance in each pore was calculated numerically using the collocation scheme developed by Tilton and Payatakes (1984). The nodal pressure values were then determined by solving the mass bal-

ance equation at the network sites. Thus, having calculated the local flow field within each cell, fully 3-D particle trajectory calculations were performed taking into account the forces and torques mentioned above. The impacted fraction in each cell was calculated based on the loci of critical particle entrance positions that lead to capture at the pore exit mouth (limiting trajectories). Finally, the particle population balance equation complemented by the perfect mixing equation of outgoing streams at every node of the network formulated a set of linear algebraic equations that were solved for the nodal particle concentration values. Numerical results obtained for various values of the particle, pore mouth and pore constriction sizes were in agreement with the experimental observation that deposition in flow conduits not aligned with the macroscopic flow direction contributes substantially to the overall deposition rate. The increased collection capacity of oblique pores results from the concurrence of the lateral (to the pore axis) direction of gravity, which makes traveling particles drift towards the pore surface, and of the relatively weak drag force in the pore axis direction caused by the decreased flow rates in such cells. A complete parametric study of particle transport and deposition in 3-D sinusoidal pores (Burganos et al., 1993) revealed that the rate of deposition is heavily affected by gravity and hydrodynamics. On the contrary, the deposition rate appears insensitive to the precise value of the parameter groups that enter the calculation of the electrokinetic and London forces, as long as each of them is larger or smaller than a critical value across which a sharp change in the capture rate value of several orders of magnitude is obtained.

A practical problem that arises when the aforementioned depth filtration simulator is applied to multimodal or continuous pore-size distributions encountered in actual beds is the large amount of numerical computations required for the determination of the loci of critical particle entrance positions that lead to limiting capture and for the estimation of the impacted fraction in *each unit cell* of the network. In addition, extension of the method to transient filtration modeling would require adoption of the quasi-steady-state approximation in order to update the flow patterns and the concentration profile.

In the present work, a novel computer-aided simulator of depth filtration is developed which is based on the computation of network-scale trajectories of a large number of test particles. The simulator is formulated in a fashion that permits direct application to any type of pore-size distribution (continuous or discrete), avoids the calculation of limiting trajectories and impacted fraction in each unit cell, and provides an excellent basis for the incorporation of transient filtration phenomena. It is conceptually similar to the algorithm presented by Imdakm and Sahimi (1991) in that particle motion is monitored over the entire pore network and not restricted to the space of individual pores. However, in the present simulator test particles are allowed to follow *3-D trajectories* within *sinusoidal* pores and are not restricted to planar displacements within cylindrical tubes as done by Imdakm and Sahimi. Moreover, selection of pathways through the network is decided by more natural criteria than those used in earlier models. For instance, selection of a pathway according to the value of the local flow rate (Rege and Fogler, 1987, 1988; Imdakm and Sahimi, 1987, 1991) may not only provide poor estimates of the overall deposition rate for non-Brownian particles, but also prove totally inappropriate in the cases of upflow and horizontal flow filtration. Indeed, Burganos et al. (1993) demonstrated recently that particle stagnation and exclusion regions can develop in upflow pore segments, and these affect considerably the calculation of the impacted fraction and complicate the algorithm of selecting particle pathways through the pore network. The depth filtration simulator presented here incorporates a number of novel features that allow straightforward switch from downflow filtration to horizontal or upflow operation. The particle collection efficiency of downflow packed beds is compared to that of upflow and horizontal flow beds for discrete and continuous pore-size distributions and for various particle sizes. Theoretical arguments that document the need for further investigations of horizontal and upflow filtration systems are also provided here, based on the results from a large number of computer simulations.

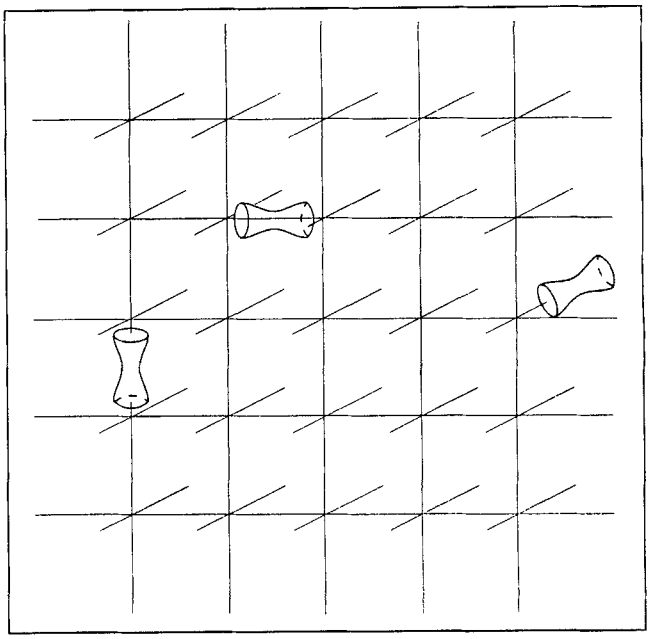

Figure 1. Portion of a cubic network of sinusoidal pores.

Description of the Simulator

A cubic network of pores with sinusoidal shape is assumed to represent the void space of a granular bed (Figure 1). Each pore or unit cell of the network is characterized by its mouth radii (R_1, R_2), constriction radius (r_c), and length (l). It is evident that all unit cells in a cubic network have the same length. However, one can easily extend the present work to distorted cubic networks or other 3-D networks of sinusoidal pores with generally varying pore length. The mouth and constriction sizes are sampled from prescribed chamber and throat-size distributions, respectively. In this way, account is taken of the actual converging-diverging geometry of the pore space in a quantitative manner although the exact local geometry is not fully simulated. Virtually any type of pore-size distribution can be used. In fact, it will become clear that the present simulator is applicable with equal facility to all types of size distribution, discrete or continuous, despite the high degree of sophistication involved in the particle motion simulation. Although most of the basic simulation features are common in all filtration modes examined here, certain peculiarities arise in the treatment of horizontal and upflow filtration, which

would confound a unified simulator description. Downflow, upflow, and horizontal flow modes are discussed separately in this order.

Downflow filtration

Test particles are injected into the pore network through the top face of the sample. The selection of the boundary pore that will admit a non-Brownian test particle is accomplished through a Monte Carlo procedure, using the fact that the probability of entrance into a pore segment is proportional to the actual transport rate of particles in that pore. All test particles are identical since they are used for the simulation of filtration of a single particle size. It is assumed that the suspensions are sufficiently dilute to exclude interparticle interactions and that the particle size to pore constriction size ratio, a_p/r_c, is sufficiently small so that the carrier flow is unaffected by the particle motion. Consequently, extension to treatment of polydispersed suspensions is straightforward and requires a simple repetition of the calculations for each particle size. In the context of the simulator presented here, which pertains to monodispersed suspensions or to a single particle size for polydispersed suspensions, the notions of reduced particle mass- and number-based concentrations are equivalent as those of reduced particle mass- and number-based fluxes.

The particle entrance rate into a unit cell is calculated using a force balance on the test particle at the pore mouth. Four types of forces are assumed to act on the particles: gravitational, hydrodynamic (including correction factors that account for particle-wall hydrodynamic interactions), London–van der Waals (including the retardation correction factor), and double ionic layer forces. Since the last two (surface) forces are too short-ranged to affect the rate of particle entrance into the pore, one can calculate the particle entrance velocity in the pore axis direction from a simple force balance involving gravity and the z-component of the drag force and, subsequently, estimate the particle injection rate into the ith pore from the expression:

$$\dot{N}_i = C_0 \int_0^{R_i - a_p} 2\Pi (v_z + u_\infty) r \, dr \qquad (1)$$

assuming for simplicity that one of the three main directions of the cubic networks coincides with the macroscopic flow direction (vertical in the downflow case). In Eq. 1 $v_z(r)$ is the component of the fluid velocity in the mean flow direction within the pore, C_0 is the inlet concentration (common for all the entrance unit cells), and $u_\infty = 2(\rho_p - \rho)a_p^2 g/9\mu$ is the limiting fall velocity with ρ_p and ρ being the particle and liquid densities, respectively. The local flow field is calculated in the following manner. The flow conductance in each unit cell is obtained through the collocation solution of the creeping flow equation in axisymmetric sinusoidal cells presented by Tilton and Payatakes (1984). Subsequent solution of the fluid mass balance equation written at each node of the network provides the nodal pressure values which, in turn, are used for the calculation of the local (axial and radial) velocity within each pore segment. The particle transport rate is then obtained from Eq. 1 and is used for the calculation of the probability of particle entrance in this pore. Note that this pore selection procedure reduces to the random selection procedure used in previous simulations of similar type (for instance, Rege and Fogler, 1988; Imdakm and Sahimi, 1991) only in the limiting case of uniform mouth and constriction sizes where all the unit cells are identical.

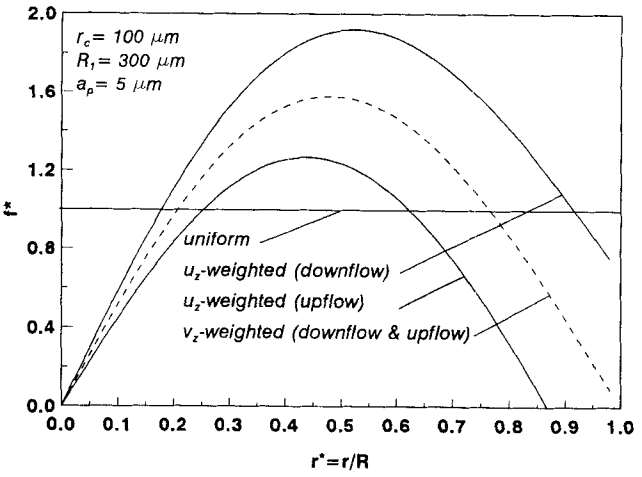

Figure 2. Number density of test particles entering a downflow unit cell.

$v_0 = 0.22$ mm s^{-1}; $u_\infty = 0.03$ mm·s^{-1}; $a_p = 5$ μm. All other parameter values from Table 1.

Once the entrance unit cell is selected, the exact entrance position within the pore mouth is selected. A uniform deviate, d_u, is generated using a pseudo-random number generator, and the radial coordinate, r_{in}, of the particle entrance is calculated numerically from:

$$d_u = \int_0^{r_{in}} (v_z + u_\infty) r \, dr \Big/ \int_0^{R - a_p} (v_z + u_\infty) r \, dr \qquad (2)$$

The angular coordinate, θ, of the particle entrance is selected randomly. In this manner we accomplish weighting of the particle entrance position according to the local (within the pore mouth) particle mass rate. Again, this novel Monte Carlo procedure is a significant improvement over the simplistic approach undertaken in earlier models which assumed a uniform distribution of particle entrance positions. Figure 2 shows the normalized density function of particles, f^*, that enter a vertical downflow sinusoidal pore. The top solid curve is obtained using the particle mass rate weighting procedure (Eq. 2) for downflow pores:

$$f^* = \frac{d\dot{N}(r)/\dot{N}(R)}{dr/R} = \frac{rR\, u_z(r)}{\int_0^{R - a_p} u_z(r) r \, dr}$$

Table 1. Parameter Values used in the Trajectory Calculations

$r_c = 100$ μm	$N_{Ret} = 314.2$
$R_1 = R_2 = 300$ μm	$N_G = 0.02258$
$l = 1{,}000$ μm	$N_{El} = 53.10$
$\psi_{01} = -30$ mV	$N_{DL} = 1{,}400$
$\psi_{02} = -8$ mV	$N_{Lo} = 5.83 \times 10^{-5}$
$\kappa = 2.8 \times 10^8$ m^{-1}	$N_{RS} = 5 \times 10^{-3}$
$H = 5 \times 10^{-20}$ J	

where $\dot{N}(r)$ is the rate of injected particles at positions with radial coordinate smaller than r. The bottom solid curve refers to the upflow case using the same procedure and will be discussed later in the corresponding subsection. The dashed curve is obtained when the particle entrance position is weighted according to the local flow field and is common to downflow and upflow pores:

$$f^* = \frac{rR\, v_z(r)}{\int_0^R v_z(r) r\, dr}$$

The horizontal straight line corresponds to the case of unweighted, random selection of entrance position (as done, for instance, by Imdamk and Sahimi, 1991). The effects of the simplified (unweighted and fluid-flow-weighted) approaches on the predicted value of the filter coefficient will be quantified and analyzed in the results and discussion section.

The particle entrance position at the pore mouth serves as the starting point for a particle trajectory within the pore. We adopt here the 3-D trajectory analysis algorithm developed by Paraskeva et al. (1991) which is outlined next. Each test particle can translate, under the action of gravity, the hydrodynamic force, the London–van der Waals force, and the electrokinetic force. It can also rotate, especially in the vicinity of the pore wall due to the hydrodynamic interaction with the surface. Starting with the force and torque balances, one can develop 3-D particle trajectory equations in the form of ordinary differential equations, which can be integrated using a standard numerical scheme (such as fourth-order Runge-Kutta). Unless the entrance position lies on the central vertical plane of the pore (that is, the vertical plane that contains the pore axis), the particle undergoes angular displacement in addition to the radial and axial ones. Sample 3-D (capture, limiting, and escape) trajectories in a horizontal unit cell are shown in Figure 3a and 3b (there parameter values from Table 1). The 3-D character of particle trajectories in nonvertical cells has been overlooked by previous investigators (Imdakm and Sahimi, 1991) who restricted the motion of the particles on vertical planes and neglected angular displacement.

If the trajectory of a test particle within a unit cell leads to contact with the pore wall, it is assumed that the particle is captured at that position (one-step trajectory method), and its trajectory is terminated. The coordinates of the capture position are recorded, and a new test particle is injected into the working sample. If the particle escapes capture in the unit cell, it arrives at a pore intersection and enters an adjacent pore segment to continue its travel. Again, various approaches have been used in the literature for the selection of the new pore including random walk (equal probabilities of entrance into all the adjacent pores) and flow-rate-biased selection (probability proportional to the local flow rate). The rigorous procedure, however, is to select the pore segment with probability proportional to the local particle mass rate. This procedure is employed here. Although the significance of this choice of pore selection procedure is not directly evident for downflow operation, it will become apparent later in this section that the particle mass-rate-weighted pore selection procedure is indispensable in the simulation of horizontal flow and upflow filtration. Once the pore segment is selected, an entrance position is assigned to the particle using the aforementioned Monte Carlo procedure (Eq. 2) that weights the radial coordinate of entrance by the local particle mass rate. 3-D particle trajectory calculations are then performed which can lead to capture or to escape, and so on. If the particle escapes through one of the lateral faces of the network sample (through a face parallel

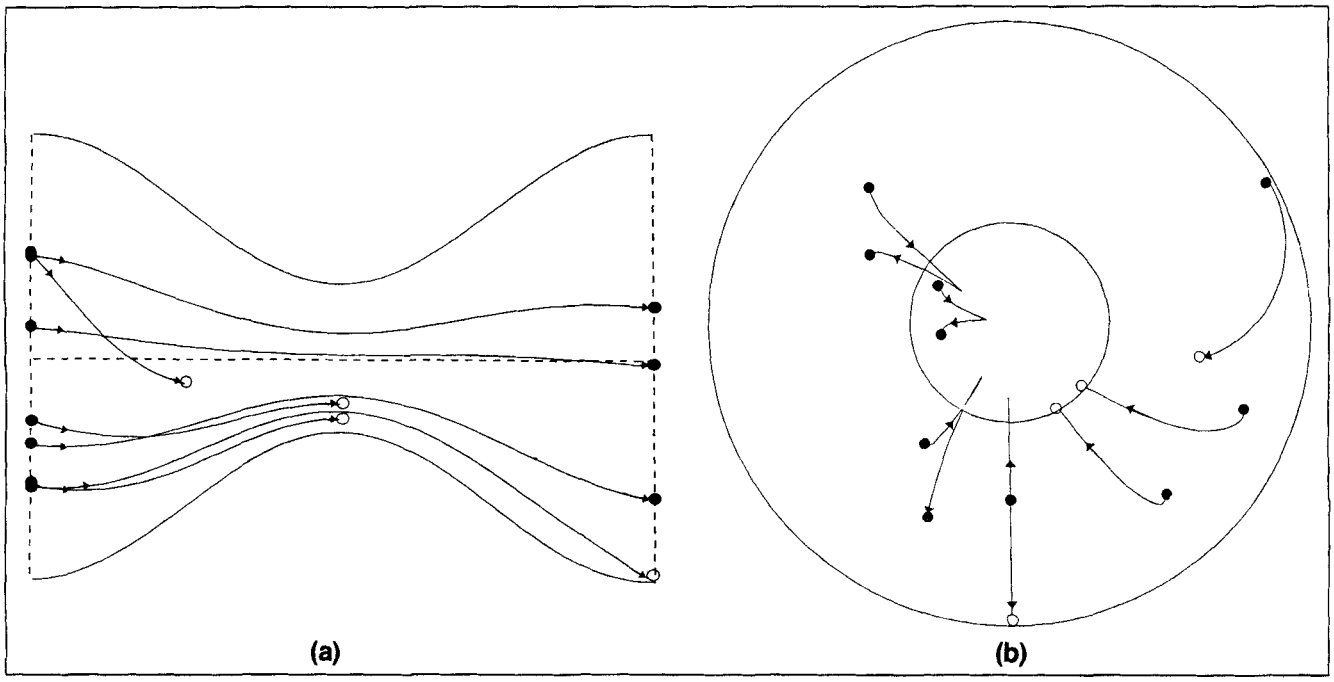

Figure 3. (a) Side- and (b) cross-sectional views of escape, limiting, and capture trajectories in a horizontal unit cell.

Void circles indicate capture; $v_0 = 0.22$ mm s^{-1}; $a_p = 5$ μm. All other parameter values from Table 1.

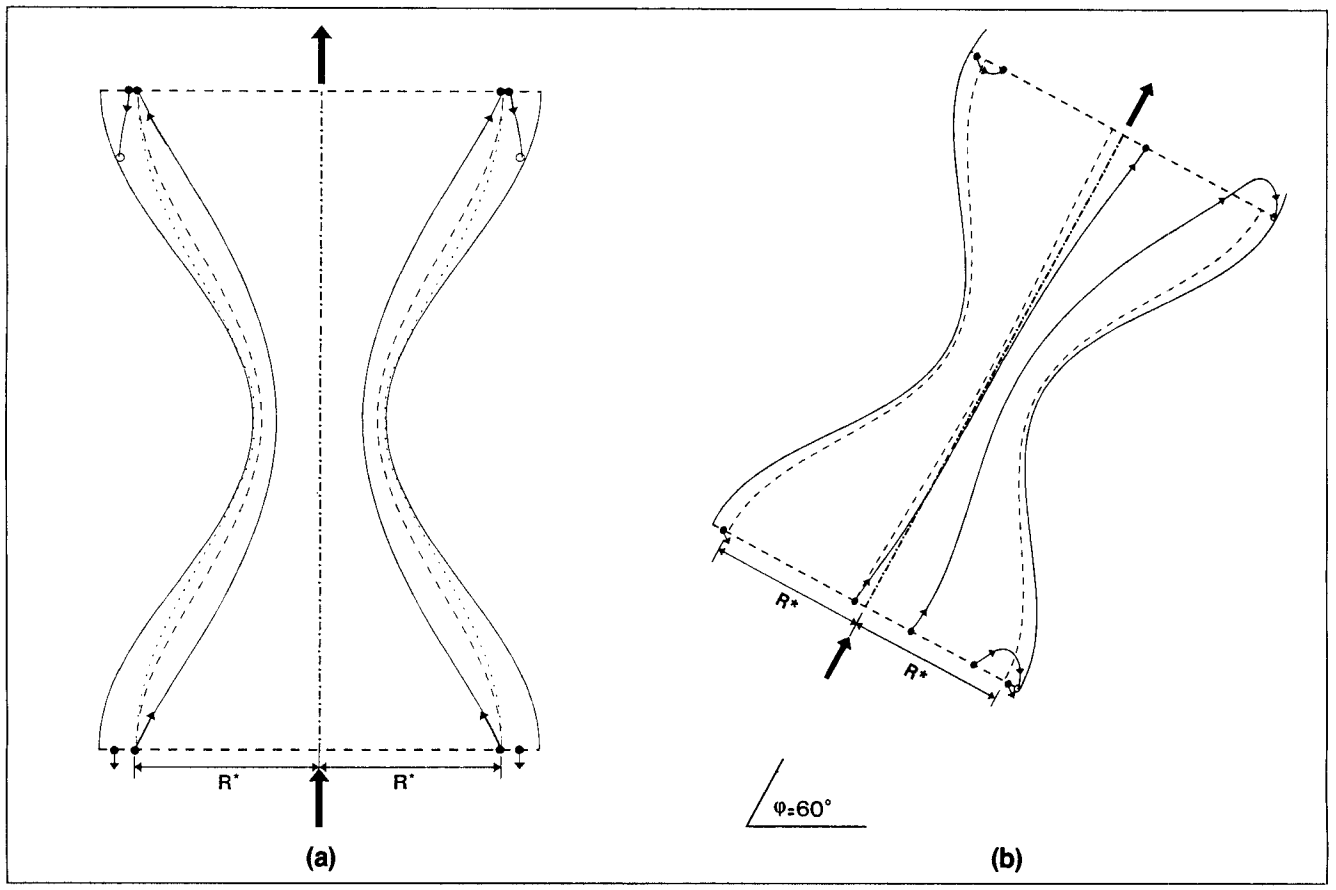

Figure 4. Locus of particle stagnation points (···), limiting capture and escape trajectories (——), and corresponding streamlines (---) in upflow (a) vertical and (b) inclined unit cells.

$r_c = 90$ μm; $a_p = 5$ μm; $v_0 = 0.75$ mm·s^{-1}. All other parameter values from Table 1.

to the mean flow direction), the particle is reinjected into the medium through an identical unit cell at the opposite face of the sample, in accordance with the structure periodicity adopted in our simulations. If the particle escapes through the exit face of the sample, it is considered transmitted and its trajectory is terminated.

Upflow filtration

In the simulation of upflow filtration the test particles are injected into the working sample through the bottom face in a fashion similar to that described above in the downflow case. However, certain complications arise in the calculation of the particle mass rate into the boundary unit cells, which are caused by the competition of gravity and hydrodynamics. Particle stagnation and exclusion regions can develop at the entrance mouth of the cells (Figure 4), the extent of which is a strong function of the particle size and density, flow rate, and cell geometry. Consequently, particles can enter upflow cells through the allowed regions only, and not through the entire pore mouths, as happens with downflow and horizontal flow cells. If the particle escapes capture in a boundary unit cell, it arrives at a pore intersection and enters an adjacent segment with probability proportional to the local particle mass rate. It may also occur that a particle entrance region can develop at the top mouth of an upflow cell. Particles can enter an upflow cell (moving downwards) at positions near the pore wall, where the fluid velocity is sufficiently small. Care is taken to treat correctly such double entrance—double exit unit cells, which may also appear during horizontal flow filtration. For a detailed analysis of particle transport and deposition in upflow cells refer to the article by Burganos et al. (1994). The upflow filtration simulation proceeds in all other respects in a fashion that is identical to that followed in the downflow simulation.

Horizontal flow filtration

The simulation of horizontal flow filtration is implemented in a manner that is similar to that described in the upflow case. Thus, one must take into account the possible existence of upflow unit cells and the double entrance—double exit phenomena that may develop therein. An additional peculiarity that appears during horizontal flow filtration is a gravity caused particle drift towards the bottom side of the bed (perpendicular to the bed axis), the magnitude of which depends heavily on the particle size and density, the superficial velocity, and the type of packing. In our simulations this particle drift can be estimated by the ratio of the average vertical displacement to the displacement in the mean flow direction. This drift implication is safely circumvented by our simulator thanks to the structure periodicity employed here. However, such a particle

drift would destroy the particle concentration and flux periodicity in population-balance-based methods and would require a different treatment which falls beyond the scope of this work.

Calculation of the Filter Coefficient

The expression:

$$\left(\frac{\partial C}{\partial z'}\right)_{\tau} = -\lambda C \tag{3}$$

suggested by Ives (1960) is used here for the definition and estimation of the filter coefficient of a packed bed. In Eq. 3 z' is the axial coordinate within the bed, C is the average particle concentration at z', and τ is time. At the initial filtration stages $\lambda(=\lambda_0)$ is not a function of the axial distance z', and Eq. 3 yields upon integration (from entrance to exit):

$$\lambda_0 = -\frac{1}{L}\ln\frac{C_{\text{eff}}}{C_0} \tag{4}$$

where C_0, C_{eff} are the influent, effluent stream concentrations, respectively, and L is the length of the bed. It is trivial to show that the λ_0 value can be obtained from our simulations using the expression:

$$\lambda_0 = -\frac{1}{m_z l}\ln f_{\text{esc}} \tag{5}$$

where m_z is the number of unit cells in the working sample parallel to the mean flow direction, l is the length of each unit cell, and f_{esc} is the number fraction of test particles that escape through the exit face of the sample.

In the particular case of unimodal pore-size (mouth and constriction) distribution certain interesting analytical results can be derived for the clean filter coefficient. In the cases of downflow and upflow operation, flow occurs only within vertical cells, the pressure drop in horizontal pores being identically nil. Since gravity is also acting in the vertical direction, the motion of the test particles is restricted to the space of vertical pores only. It is easy to see that the filter coefficient in the upflow and downflow filtration cases is given by the following expression for unimodal structures:

$$\lambda_0 = -\frac{1}{l}\ln f_0 \tag{6}$$

where f_0 is the number fraction of particles that escape through each vertical unit cell. Note that the λ_0 value as predicted by Eq. 6 is independent of the size of the network sample (as it should).

However, in the horizontal flow filtration case particles can actually enter unit cells that are perpendicular to the mean flow direction even in the unimodal limit. Particles can assume trajectories (capture or escape) within vertical cells despite the lack of fluid flow in them (sedimentation), driven at the pore entrance only by gravity. As the particle starts its descent, the Stokes hydrodynamic resistance develops and in the vicinity of the pore surface hydrodynamic interactions, as well as surface forces (London–van der Waals and electrokinetic), come into play. It can be shown by a rigorous analysis that the clean filter coefficient in unimodal horizontal flow filters (with one family of pores parallel to the mean flow direction, one vertical, and the third horizontal) is given by the expression:

$$\lambda_0 = -\frac{1}{m_z l}\ln\frac{1}{m_x - 1} f_z^{m_z}\left\{\dot{n}_z^{m_z-1}\sum_{i=1}^{m_x-2}\left[1+\sum_{j=1}^{i-1}\times\binom{m_z+j-2}{m_z-2}(f_x\dot{n}_x)^j\right] + \sum_{i=1}^{m_z-1}\left[\dot{n}_z^{i-1}\sum_{j=0}^{m_x-3}\binom{i+j-1}{i-1}(f_x\dot{n}_x)^{j+1}\right]+1\right\} \tag{7}$$

where m_z is the number of cells in the mean flow direction (horizontal), m_x is the number of cells in the vertical direction, f_x, f_z are the escape probabilities in the x- and z-directions, respectively, and $\dot{n}_x$, $\dot{n}_z$ are the fractions of particle mass that exit from a pore intersection and enter the x- or z-directed cell, respectively. It must be noted that Eq. 7 has been derived using periodicity in the horizontal direction only (that is normal to the mean flow direction). The bed-scale "sense anisotropy" induced by the action of gravity prohibits periodicity in the vertical direction and the actual physical boundaries of the bed must be defined. To this end, the assumption of impermeable horizontal wall has been used. This problem is absent in the test-particle-based simulations where neither particle concentration nor particle transport rates need to be determined. Each time a test particle crosses a lateral face of the working sample, it is reinjected into the sample through the opposite face thanks to the geometric periodicity of the pore network, and continues its travel. It is only the particle displacement in the mean direction of flow that is of interest in the filter coefficient simulations, the recording of the particle motion in transverse directions being useful for dispersion calculations only or to ensure that the horizontal bed walls are not intercepted.

Results and Discussion

The simulation results for downflow and horizontal flow unimodal filters are presented first (Figure 5). (Throughout this section, unless otherwise stated, horizontal flow filters are assumed to have one family of pores in the vertical direction.) The marked points correspond to results that were obtained through test particle-based Monte Carlo computation of escape probabilities in individual horizontal and vertical pores followed by use of Eqs. 6 and 7 for the calculation of the (clean) filter coefficient. The solid lines correspond to results that were obtained using the limiting trajectory concept for the calculation of the impacted fraction, η, in the unit cells (Burganos et al., 1993):

$$\eta = \frac{\iint_{A_c} u_z(r,\theta) C_0 r\, dr\, d\theta}{\iint_{A_o} u_z(r,\theta) C_0\, r\, dr\, d\theta} \tag{8}$$

followed again by use of Eqs. 6 and 7 with $f = 1-\eta$ (escape probability) for the calculation of the filter coefficient. In Eq.

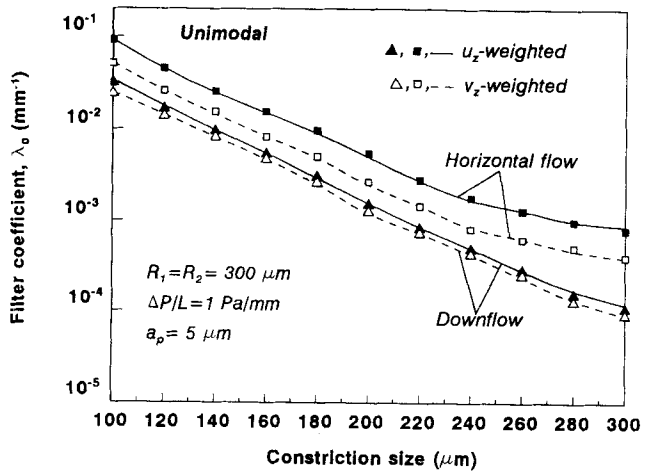

Figure 5. Filter coefficient predictions of test particle (marked points) and population balance (curves) methods for unimodal filters with varying constriction sizes.

Comparison of the horizontal to downflow modes and of particle- (filled markers, solid curves) to fluid- (void markers, dashed curves) weighted computations. Parameter values other than those shown in the graph from Table 1. Network size: $20\times20\times20$.

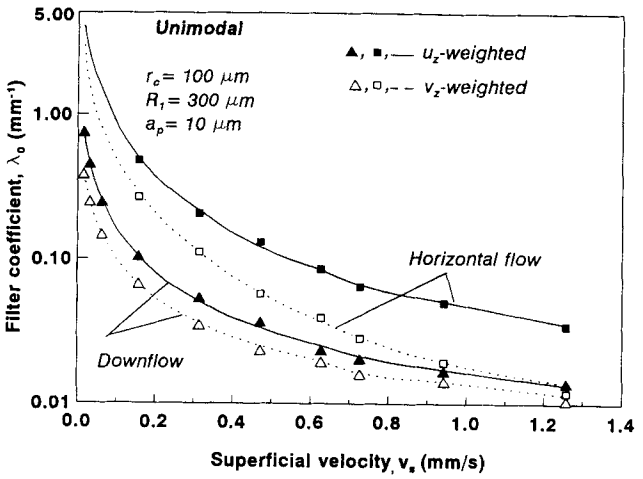

Figure 6. Dependence of the horizontal and downflow unimodal filter coefficient on superficial velocity using the test particle (marked points) and the population balance (curves) methods.

Comparison of the particle- (filled markers, solid curves) to fluid- (void markers, dashed curves) weighted computations. Parameter values other than those shown in the graph from Table 1. Network size: $20\times20\times20$.

8 A_c is the region of entrance positions that lead to particle capture, and A_o is the actual particle entrance region of the pore mouth. Note the excellent agreement between the filter coefficient results, as predicted by the limiting trajectory method, and the results obtained by the test particle approach, which essentially provides statistical estimates of the righthand side of Eq. 8. (It was found that use of a few thousand test particles provided sufficiently accurate results.) Hence, any possible statistical error should be probably attributed to the finite dimensions of the working sample and not to the selection of either computational technique. Extensive experimentation on the sample size showed that $20\times20\times20$ networks constructed with structural periodicity provided statistically accurate filter coefficient estimates. All the results presented in this work were obtained using this network size and averaged over three different realizations. The deviations of the results for the different realizations were almost always too small to mention and, consequently, use of error bars in the graphs was avoided. On the contrary, if the older definition of η is employed, which uses the fluid velocity $v_z(r,\theta)$ in place of the particle velocity $u_z(r,\theta)$ in Eq. 8, the λ_0 results shown by the dashed lines in Figure 5 are obtained which are clearly lower than the actual ones. This underestimation of the impacted fraction and of the filter coefficient stems from the fact that use of the fluid velocity in the η calculation biases the particle entrance towards the pore axis and, therefore, towards the high velocity region of the pore. It is also remarkable that use of straight cylindrical pores leads to filter coefficient values that can be two (or more) orders of magnitude lower than those obtained when constricted pores are used. Upflow operation under the conditions used in this figure would give a much larger than gravity hydrodynamic drag, and would lead, consequently, to the elimination of stagnation and double entrance regions. Since the capture efficiency of upflow vertical cells is almost nil, the upflow filter becomes under these conditions practically inactive.

Downflow and horizontal flow filter coefficient values are plotted against the superficial velocity for unimodal filters in Figure 6. Marked data are Monte Carlo estimates of the filter coefficient based on the particle transport-rate-weighted (top curves in each flow mode) and on the fluid-flow rate-weighted (bottom curves in each flow mode) selection of pore segments and of particle entrance positions at pore mouths. The corresponding λ_0 predictions of the population balance method that uses limiting trajectory-based calculations of the impacted fraction in each direction are shown by the solid (particle-weighted) and dashed (fluid-weighted) curves of the same figure. The excellent agreement of the two approaches verifies our conception that the test particle method provides statistical solutions to the population balance equations and to the impacted fraction equation (Eq. 8). However, care must be taken so that the same criteria for the pore segment selection at intersections and for the particle entrance position selection at pore mouths are used in the two approaches. It is also interesting to note that the filter coefficient in both flow modes decreases rapidly with increasing superficial velocity (or equivalently with increasing macroscopic pressure drop in the mean flow direction).

Figure 7 shows the dependence of the unimodal filter coefficient on the particle size in the horizontal and downflow cases. Here, we have used the same data representation fashion as that in Figure 6 (markers for the Monte Carlo estimates and curves for the population balance-based predictions). The agreement of the test particle and population balance approaches is again excellent over the entire particle-size range considered. Note that increasing the particle size from 1 μm to 30 μm causes a filter coefficient increase by more than two orders of magnitude for the particular set of data used in this figure. (However, it should be stressed that numerical results for particle sizes that are nonnegligible compared to the pore size—larger than about 20 μm in this particular graph—should be regarded with some reservation and serve as trend indica-

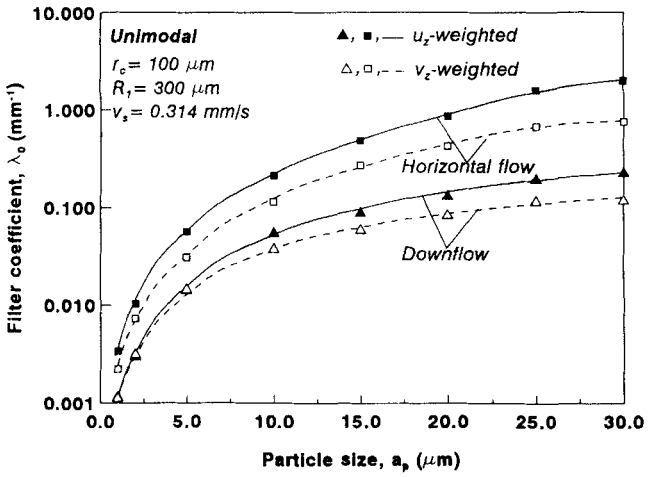

Figure 7. Dependence of the horizontal and downflow unimodal filter coefficient on particle size using the test particle (marked points) and population balance (curves) methods.

Comparison of the particle- (filled markers, solid curves) and fluid- (void markers, dashed curves) weighted computations. Parameter values other than those shown in the graph from Table 1. Network size: 20×20×20.

tions rather than as exact quantitative information.) It is also noteworthy that the deviation of the particle- and fluid-based approaches (top and bottom curves in each flow mode) increases with increasing particle size, as expected. Direct comparison of the downflow and horizontal flow filter performances shows that for particle sizes larger than 20 μm the horizontal flow filter coefficient becomes more than one order of magnitude larger than that in the downflow mode. Considering the exponential relation between the filter coefficient and the effluent concentration (see Eq. 4), it can be deduced that horizontal flow operation can yield filtrates of highly improved clarity compared to that obtained during downflow operation for uniform packings.

Concentration profiles at different depths within unimodal horizontal flow filters are shown in Figures 8a and 8b. The concentration ratio c/c_{top} is plotted in Figure 8a vs. the distance from the top face of the filter (expressed as number of unit cells from the top wall), where $c = c(x,z)$ is the particle concentration at the node (x,z) (concentration of outgoing streams at that node), and $c_{top} = c_{top}(z)$ is the concentration of the top node of the corresponding vertical unit bed column. Note the considerable variation of nodal concentration with the distance from the top wall, which is progressively amplified at larger depths (measured in unit cells from the filter entrance). These interesting concentration profiles, which are intuitively quite reasonable for horizontal flow operation, could have never been predicted by the flow rate-weighting approach. This approach restricts particle transport and deposition in horizontal pores only (where fluid flow occurs) and predicts constant concentration, $c_f(z)$, within each unit bed column. This depth-dependent concentration, $c_f(z)$, is compared in Figure 8b to the exact local concentration, c, as that is predicted by the particle transport-rate-weighting method at various distances from the top wall of the horizontal flow filter and at various depths measured in unit cells. The tremendous deviation of the predictions of the two methods, which becomes explosively

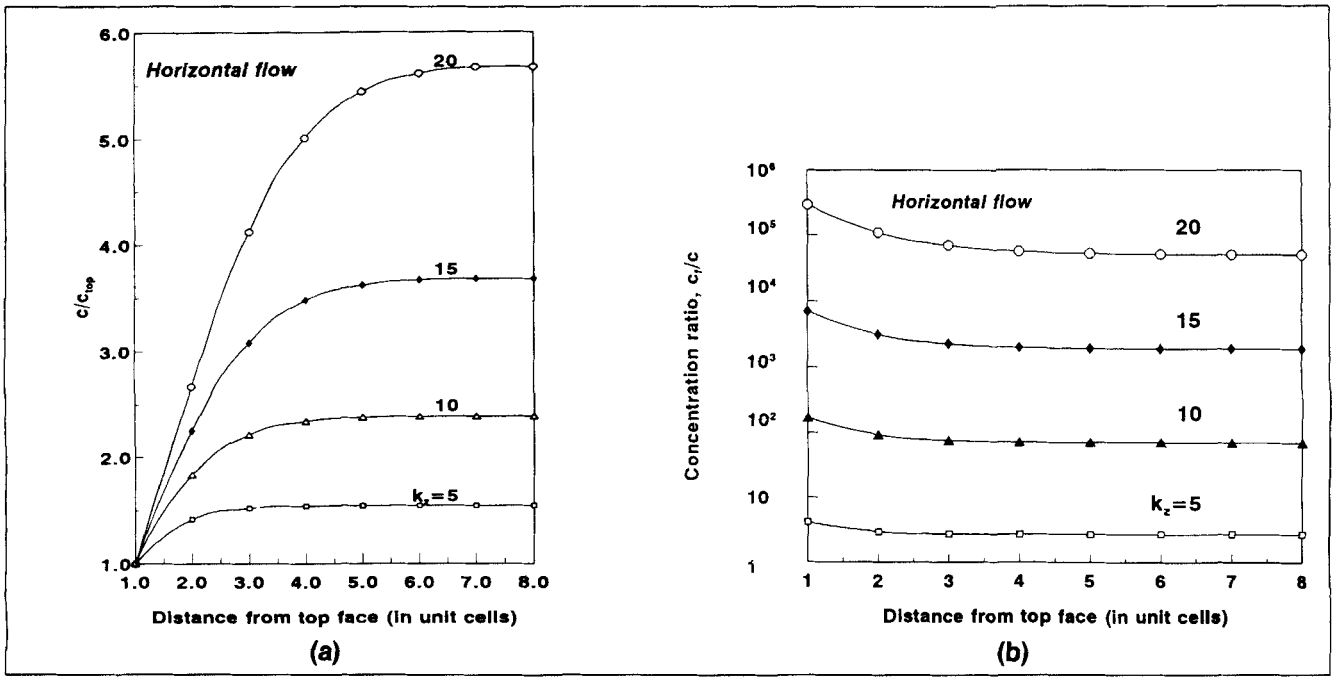

Figure 8. Nodal concentration profiles.

(a) Ratio of nodal concentration to concentration at top node of the corresponding vertical unit bed column vs. distance from the upper face of a network with unimodal constriction size distribution at various depths, k_z. All distances are measured in unit cells. (b) Ratio of nodal concentration obtained by fluid-weighting to concentration based on particle-weighting vs. distance from the upper face of a network with unimodal constriction size distribution at various depths, k_z. All distances are measured in unit cells. Parameter values other than those shown in the graphs from Table 1.

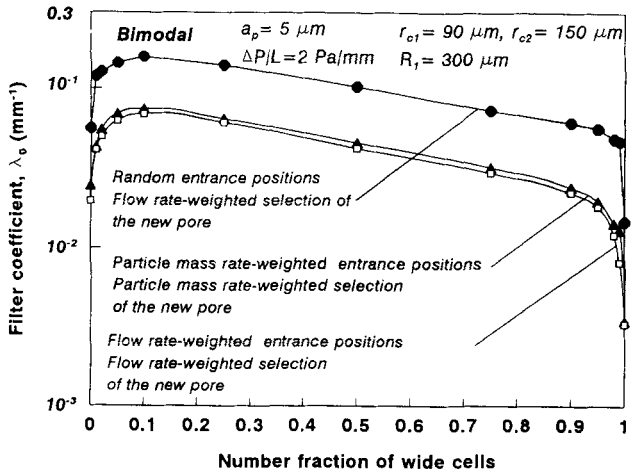

Figure 9. Downflow filter coefficient vs. number fraction of wide cells for strictly bimodal constriction size distribution.

Comparison of the different weighting procedures. Parameter values other than those shown in the graph from Table 1. Network size: 20 × 20 × 20.

large only 15–20 unit cells away from the entrance for the data used in this figure, is attributed solely to particle sedimentation within the vertical pores. This sedimentation phenomenon is entirely neglected by the flow-rate-weighting approach. The deviation of the two sets of results is a strong function of the wall geometry, the local flow rate, and the particle size (see Figures 5–7 and the relevant discussion).

Downflow filter coefficient estimates in the case of uniform mouth size and strictly bimodal distribution of the constriction size are shown in Figure 9 against the number fraction of wide unit cells (cells with the larger constriction). The intermediate curve is a least-square fit of the results (marked points) obtained by the test particle simulator developed in this work. The bottom curve is obtained when the selection of pore segments at intersections and of particle entrance positions at pore mouths is local flow rate-weighted instead of particle mass-rate-weighted. This approach is conceptually identical to the population balance method developed by Burganos et al. (1992), but provides a Monte Carlo solution to the set of algebraic equations that express the population balance at the network nodes and the assumption of perfect mixing within the intersection regions (which implies uniform concentration in outgoing streams). The flow rate-weighted approach biases the test particles towards the pore axis where relatively high velocities develop and, consequently, underestimates the actual filter coefficient. On the other hand, the simplified approach taken by Imdakm and Sahimi (1991), which biases the test particles towards high flow rates at pore intersections and injects particles into selected pores in a totally random fashion (uniform distribution of entrance positions over the pore mouth), appears to overestimate the actual filter coefficient considerably. The reason for this failure lies in the fact that a significant portion of particles enters through the low velocity region near the pore wall (Figure 2) and is, therefore, biased towards the pore surface and, finally, led to deposition. At the lower unimodal limit (the pore space is made up of narrow cells exclusively) fluid flow and particle transport occur through the vertical cells only. Introduction of a small number of wide cells activates the horizontal unit cells and leads to higher filter coefficients despite the fact that the wide cells are less efficient collectors than the narrow ones. At the upper unimodal limit (exclusively wide cells), fluid flow and particle transport are again restricted to within the vertical cells only, which are relatively poor collectors, and, therefore, the filter coefficient becomes smaller than that obtained at the lower unimodal limit.

A direct comparison of the performance of downflow, upflow, and horizontal flow filters with bimodal constriction size distribution is made in Figure 10. The ratio of the filter coefficient in the upflow and the horizontal flow modes to that during downflow filtration is plotted here against the number fraction of wide cells. Note that the horizontal flow filter performs better than the downflow one only in the vicinity of the two unimodal limits for the particular values of parameters used in this figure. As the unimodal limits are approached, the difference between the capacities of the two types of filters becomes quite large, which implies that the horizontal filter effluent clarity is far superior to that in downflow operation. On the other hand, upflow filters perform worse than downflow ones over the entire network composition range. Again, this efficiency difference becomes maximal at the two unimodal limits (nil capture efficiency of the upflow filter at the conditions of this particular case-study) and remains nonnegligible in the intermediate (mixed population) region.

The poor performance of the upflow filter compared to that of the same filter in the downflow mode (with $\rho_p > \rho$) can be explained in the following manner. Particle capture efficiencies of horizontal pores are identical in the two types of operation. However, the vertical pores are incapable of collecting any particulate matter during upflow operation, whereas in the downflow mode they present some finite capture efficiency. Hence, the difference in the filter coefficients of the two flow modes is attributed chiefly to the collection capability of the vertical downflow pores. The explanation of the alternating performance of the horizontal and downflow filters is somewhat more complicated. At the unimodal limits, horizontal pores are inactive during downflow operation and particle deposition can take place only in the (poorly collecting) vertical pores. On the contrary, at the same limits the deposition rates during horizontal flow operation are high thanks to the combined action of the horizontal pores (which are far better collectors than vertical ones for the same pressure drop) and of the vertical pores (where highly efficient sedimentation occurs). However, as a second type of pores is introduced into the network (mixed population range) fluid flow develops in each pore segment during both types of operation rendering the two modes of comparable efficiency. The (reduced) performance of horizontal flow filters in the intermediate population region is strongly influenced by the superficial velocity (or, equivalently, by the macroscopic pressure drop along the bed). Figure 10b reveals that decreasing the pressure drop, $\Delta P/L$, improves the horizontal flow filter performance relative to that during downflow operation over a progressively wider population range. For sufficiently low values of $\Delta P/L$, the horizontal flow mode becomes superior to the downflow one for any network composition. This is expected, considering that downflow filtration becomes almost gravity-driven for small values of the superficial velocity thus deactivating the otherwise highly efficient horizontal pores. On the other hand, gravity drives the

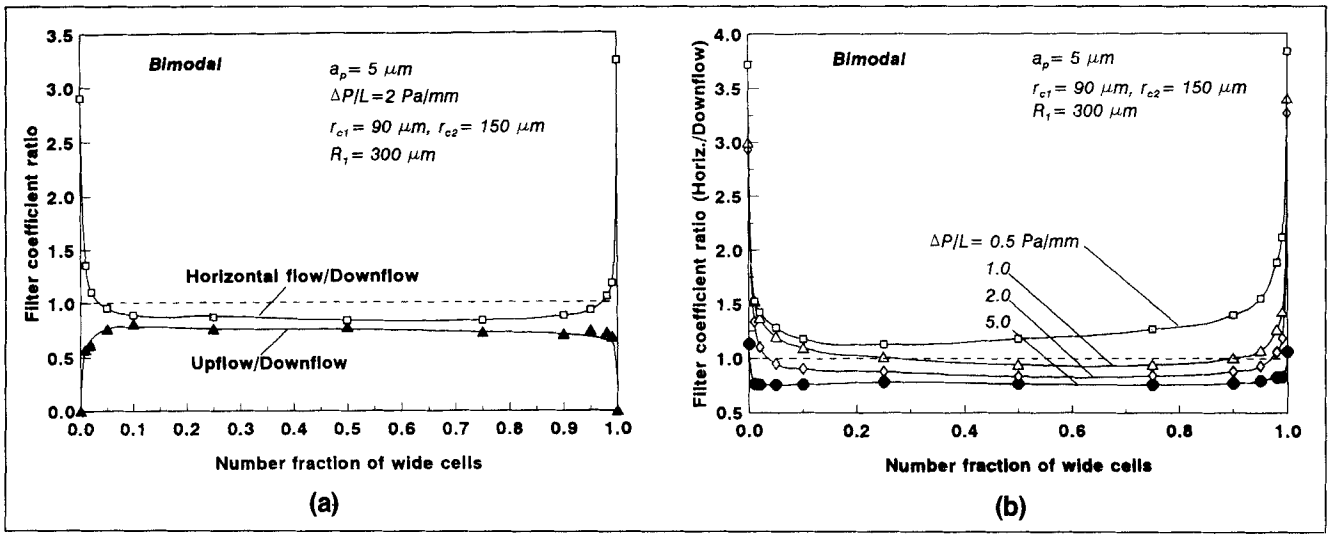

Figure 10. Comparison of flow modes.

(a) Horizontal flow to downflow and upflow to downflow filter coefficient ratios vs. number fraction of wide cells for strictly bimodal constriction size distribution. (b) Horizontal flow to downflow filter coefficient ratio vs. number fraction of wide cells for strictly bimodal constriction-size distribution. Variation with the externally applied pressure drop. Parameter values other than those shown in the graphs from Table 1. Network size: 20×20×20.

particles that enter a horizontal flow filter to direct deposition on the surfaces of the boundary (and neighboring) horizontal pores, thus increasing drastically the capture capacity.

Figure 11 shows the variation of the number fractions of escaping particles and of deposited particles with the length of the pathway followed to the exit face of the network or to capture by some internal pore surface, respectively, expressed as number of cells making up the path, N_c. The figure refers to downflow operation in the case of strictly bimodal distribution of the constriction size. Wide and narrow cells are distributed throughout the network with equal probabilities. Note that the residence time distribution for captured particles presents a sharp peak at $N_c=2$, which corresponds to the top layer of horizontal unit cells. It is also interesting to note that the mean travel distance of escaping particles within the network sample is roughly 33% larger than their displacement in the mean flow direction. This is a simple measure of the particle dispersion during downflow filtration. Moreover, this type of information is particularly useful in applications that involve flow of suspensions of biological matter through porous media. In this case, increased residence times can lead to early pore clogging if the feed suspension contains sufficient nutrients to sustain rapid growth of the suspended organisms.

Filter coefficient calculations in the three flow modes have also been performed for lognormal constriction size distribution, which is expected to represent better an actual bed structure than previously discussed unimodal and bimodal distributions. A discretized version of a lognormal distribution has been used ($\bar{r}_c/R_1=0.5$; $\sigma/R_1=0.5$) allowing a certain degree of calculation grouping and savings of considerable computational time. The largest size that a pore constriction can attain is obviously the mouth size ($R_1=300$ μm), which results in a cutoff at $r=R_1$. The dependence of the clean filter coefficient on the superficial velocity and on the particle size for such a constriction size distribution is shown in Figures 12 and 13, respectively, for the three modes of operation. Downflow operation yields, in general, filtrates of higher clarity compared to those of both horizontal and upflow operation for the majority of superficial velocity values considered here, whereas upflow filters appear to collect less than both horizontal and downflow filters for any value of the superficial velocity and for any particle size. For small superficial velocity values ($v_s < \sim 1$ mm/s), however, horizontal flow filtration seems to perform better than downflow filtration. This behavior can be explained in the same way as that used above in the discussion of the analogous trend for bimodal constriction size distributions.

The simplified approach that uses flow-rate-biased selection of pore segments at intersections and random particle entrance

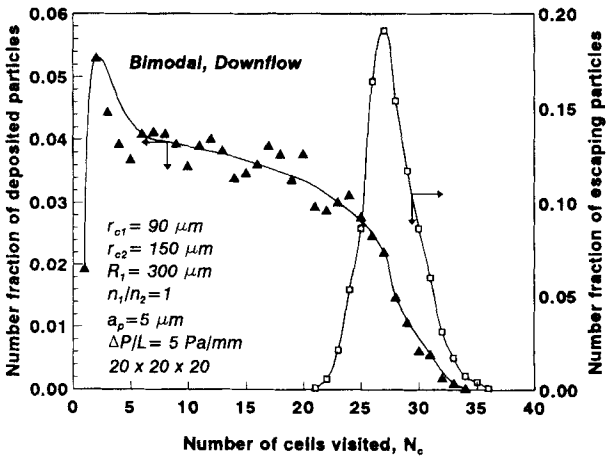

Figure 11. Number fraction of deposited/escaping particles vs. number of through cells during downflow operation in a 20 × 20 × 20 network with equal population of narrow and wide unit cells.

Parameter values other than those shown in the graph from Table 1.

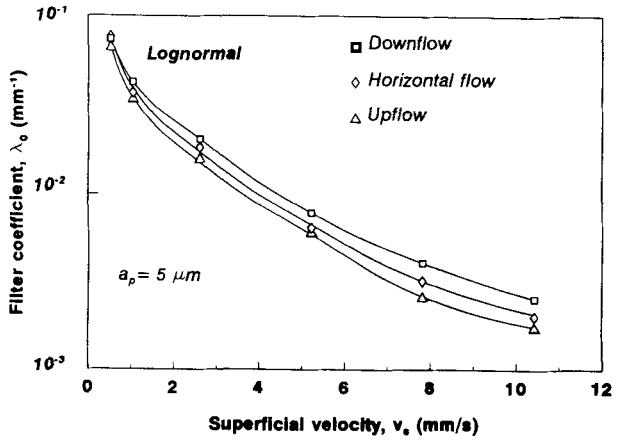

Figure 12. Dependence of the clean filter coefficient on the superficial velocity for networks with lognormal constriction-size distribution ($\bar{r}_c/R_1 = 0.5$; $\sigma/R_1 = 0.5$).

Variation with the flow mode. Parameter values other than those shown in the graph from Table 1. Solid lines are least-square fits. Network size: 20×20×20.

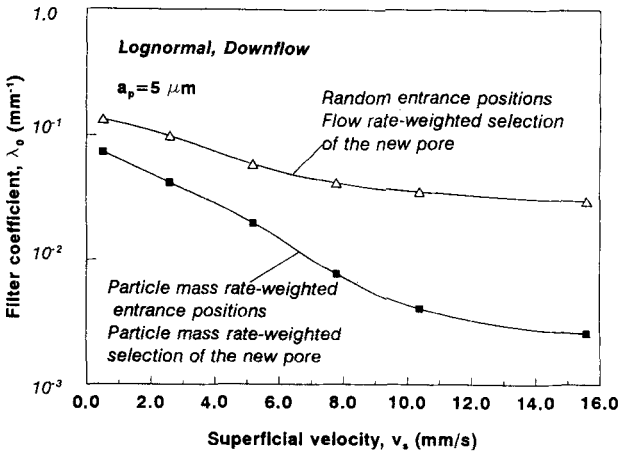

Figure 14. Downflow filter coefficient vs. superficial velocity for lognormal constriction size distribution ($\bar{r}_c/R_1 = 0.5$; $\sigma/R_1 = 0.5$).

Comparison of the exact results to the predictions of a simplified procedure for the selection of pore segment at intersections and of particle entrance position at pore mouths. Parameter values other than those shown in the graph from Table 1. Solid lines are least-square fits. Network size: 20×20×20.

positions at pore mouths used by Imdakm and Sahimi (1991) can lead to large overestimation of the actual filter coefficient even in the case of lognormal constriction size distribution, as seen in Figure 14 for the downflow mode. The increased deviation that is observed at high superficial velocities is attributed to the unrealistic particle injection procedure used in that simplified approach, which fails to distinguish between slow and fast entrance regions and introduces a considerable fraction of test particles in the vicinity of the pore wall where capture is very likely to occur, after a short path within the pore space.

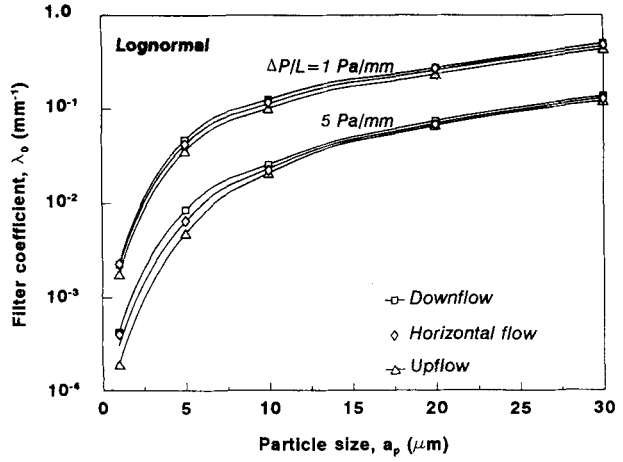

Figure 13. Dependence of the clean filter coefficient on the particle size for networks with lognormal constriction size distribution ($\bar{r}_c/R_1 = 0.5$; $\sigma/R_1 = 0.5$).

Variation with the flow mode and the externally applied pressure drop. Parameter values other than those shown in the graph from Table 1. Solid lines are least-square fits. Network size: 20×20×20.

Conclusions

A deep bed filtration simulator has been developed, capable of describing the motion and deposition of suspended particles in the interior of downflow, upflow, and horizontal flow filters and of predicting their collection efficiency at the initial filtration stages. A cubic network of sinusoidally shaped unit cells is used to represent the pore space of the filter. Although some accuracy in the simulation of actual particle trajectories is lost in the pore network approximation by potentially overlooking certain particle motion events within the pore throat interconnection space, the employment of pores with converging-diverging geometry adopted in this work is much more realistic than the oversimplified cylindrical tube approach that is usually followed in the literature. The simulation proceeds in three stages. First, a Monte Carlo procedure used for the sampling of pore (mouth and/or constriction) sizes from prescribed discrete or continuous distributions. Then, the flow conductances of all the unit cells in the network are calculated by numerically solving the creeping flow equation within sinusoidal boundaries using the collocation scheme by Tilton and Payatakes (1984). The nodal pressure values are easily calculated using the standard network analysis which involves solution of the fluid mass balance equation at the network sites. Finally, network-scale trajectories of a large number of test particles are calculated which are terminated either upon collision with some pore wall (particle capture) or upon escape through the exit face of the working sample (particle transmission or escape). The calculation of 3-D particle trajectories within the unit cells involves integration of the particle trajectory equations, derived earlier (Paraskeva et al., 1991) and account for translation and rotation of the particle under the action of hydrodynamic forces and torques, gravity, the London-van der Waals force, and the double ionic layer force. The trajectory calculations for a test particle that collides with some pore wall terminate at the collision point and the particle is assumed to stick instantaneously. If the particle escapes through a unit cell, it is injected into an adjacent pore segment

with probability that is proportional to the local particle entrance rate. This network-scale trajectory simulator offers some practical advantages over the population balance method suggested by us earlier (Burganos et al., 1992). Although the two methods are equally accurate, the tedious calculation of the impacted fraction in each unit cell of the network (required as an input to the population balance equations at the network nodes) is avoided in the test particle method treating with equal facility any type of pore-size distribution (continuous or discrete). The local deposition rate (or impacted fraction) can also be calculated, if desired, by the test particle method in a statistical manner. Comparable computational times are required by the two methods for the same degree of accuracy when simple, discrete size distributions are considered. The test particle method, however, becomes considerably less time consuming than the population balance method when networks with discrete multimodal or continuous pore-size distributions are examined. Finally, the test particle simulator can be extended in a straightforward manner to simulate transient filtration.

The selection of pore segments at intersections for the continuation of the particle trajectory as well as the selection of the particle entrance position at pore mouths are weighted according to the local particle transport rate in contrast to the customarily used flow rate-weighting approach. Numerical results presented in this article show that the flow rate-weighted procedure underestimates considerably the actual filter coefficient over a wide range of superficial velocity, and particle- and pore-size values. On the other hand, the simplistic approach of injecting test particles at totally random positions suggested earlier in literature overestimates significantly the exact filter coefficient (by one order of magnitude in some cases).

Heterogeneous downflow filters proved more efficient than both horizontal and upflow filters with the same packing and externally applied pressure drop over a broad range of parameter values. However, small superficial velocities favor the horizontal flow mode due to the gravity-dominated particle motion and the concomitant accumulation in the entrance bed region. Horizontal flow operation is also favored by homogenization of the packing for almost any value of the externally applied pressure gradient. The filtration capability of upflow depth filters was found lower (for $\rho_p > \rho$) than both horizontal and downflow filters over the entire range of parameter values examined here. This poor performance of upflow filters is solely due to the, practically, nil collection efficiency of vertical upflow unit cells. It is also important to stress that the differences in the filtration efficiencies of the three flow modes are maximal at the unimodal pore network limit and reduce considerably for nonuniform packings. However, calculations performed in this work were restricted to cubic pore networks having one set of pores oriented vertically with quite poor collection efficiency during upflow operation. It is expected that inclination of the cubic network with respect to the vertical direction or use of other network structures would yield improved upflow filters and might alter the order of relative collection efficiency of the three flow modes. Hence, before drawing conclusions regarding the performance of the various flow modes, a systematic study must be carried out of the effect of the network topology and orientation on the filter operation.

Notation

a_p = suspended particle radius, μm
A_0 = particle entrance region on a pore mouth
c = nodal concentration, m^{-3}
c_f = particle concentration obtained using flow rate weighting, m^{-3}
c_{top} = concentration at the top face of the filter (a function of depth only), m^{-3}
C = average particle concentration, m^{-3}
C_0, C_{eff} = influent and effluent stream concentrations, m^{-3}
H = Hamaker constant, J
l = length of a unit cell, μm
L = length of the bed, m
N_c = number of cells visited
N_{DL} = double-layer parameter (dimensionless)
N_{E1}, N_{E2} = first and second dimensionless electrokinetic groups
N_G = dimensionless gravitational group
N_i = particle injection rate into the ith pore, s^{-1}
$\dot{N}(r)$ = injection rate of particles at positions with radial coordinate smaller than r, s^{-1}
N_{Ret} = retardation parameter, dimensionless
N_{RS} = relative size group, dimensionless
p_i = probability of particle entrance into ith pore segment
Q_i = flow rate in ith pore segment
$Q_{i,p}$ = particle mass rate in ith pore segment
r = radial cylindrical coordinate
r_c = constriction radius of the unit cell, μm
$\bar{r}_c$ = mean constriction radius
R_1, R_2 = mouth radii of the unit cell, μm
u_∞ = limiting fall velocity, $mm \cdot s^{-1}$
u_z = particle velocity in the mean flow direction, $mm \cdot s^{-1}$
v_0 = mean entrance fluid velocity in a unit cell, $mm \cdot s^{-1}$
v_s = superficial velocity, $mm \cdot s^{-1}$
v_z = component of the fluid velocity in the mean flow direction, $mm \cdot s^{-1}$
z = axial coordinate within a unit cell
z' = axial coordinate within the bed, m

Greek letters

ΔP = pressure drop, Pa
η = impacted fraction
κ = double layer reciprocal thickness, m^{-1}
λ = filter coefficient, m^{-1}
λ_0 = clean filter coefficient, m^{-1}
μ = dynamic viscosity, Pa·s
ρ = density of liquid, $kg \cdot m^{-3}$
ρ_p = suspended particle density, $kg \cdot m^{-3}$
σ = standard deviation of lognormal distribution of constriction size
ψ_{01}, ψ_{02} = surface potential of suspended particle and grain, respectively, mV

Literature Cited

Ahsan, T., H. W. An, J. P. Buiteman, and G. J. Alaerts, "Modeling of Particle Removal in Direct Horizontal Flow Roughing Filtration," World Filtration Cong., Nagoya, Japan, p. 252 (1993).

Burganos, V. N., C. A. Paraskeva, and A. C. Payatakes, "Three-Dimensional Trajectory Analysis and Network Simulation of Deep Bed Filtration," *J. Colloid Interf. Sci.*, **148**, 167 (1992).

Burganos, V. N., C. A. Paraskeva, and A. C. Payatakes, "Parametric Study of Particle Deposition in Sinusoidal Pores of Arbitrary Orientation," *J. Colloid Interf. Sci.*, **158**, 466 (1993).

Burganos, V. N., C. A. Paraskeva, P. D. Christofides, and A. C. Payatakes, "Motion and Deposition of Non-Brownian Particles in Upflow Collectors," *Sep. Technol.*, **4**, 47 (1994).

Donaldson, E. C., B. A. Baker, and H. B. Carrol, "Particle Transport in Sandstones," SPE Conf., No. 6905, Denver (1977).

FitzPatrick, J. A., and L. A. Spielman, "Filtration of Aqueous Latex Suspensions Through Beds of Glass Spheres," *J. Colloid Interf. Sci.*, **43**, 350 (1973).

Houi, D., and R. Lenormand, "Particle Accumulation at the Surface of a Filter," *Filtr. Sep.*, **238**, 238 (1986).
Hung, C. C., and C. Tien, "Effect of Particle Deposition on the Reduction of Water Flux in Reverse Osmosis," *Desalin.*, **18**, 173 (1976).
Imdakm, A. O., and M. Sahimi, "Transport of Large Particles in Flow Through Porous Media," *Phys. Rev.*, **A36**, 5304 (1987).
Imdakm, A. O., and M. Sahimi, "Computer Simulation of Particle Transport Processes in Flow Through Porous Media," *Chem. Eng. Sci.*, **46**, 1977 (1991).
Ives, K. J., "Rational Design of Filters," *Proc. Inst. Civil Eng.* (London), **16**, 189 (1960).
Ives, K. J., "Deep Bed Filtration," in *Solid Liquid Separation*, L. Svarovsky, ed., 3rd ed.,, Butterworths, Cambridge, UK, p. 358 (1990).
Kirkpatrick, S., "Percolation and Conduction," *Rev. Mod. Phys.*, **45**, 574 (1973).
Mackie, R. I., R. M. W. Horner, and R. J. Jarvis, "Dynamic Modeling of Deep-Bed Filtration," *AIChE J.*, **33**, 1761 (1987).
Paraskeva, C. A., V. N. Burganos, and A. C. Payatakes, "Three-Dimensional Trajectory Analysis of Particle Deposition in Constricted Tubes," *Chem. Eng. Comm.*, **108**, 23 (1991).
Payatakes, A. C., C. Tien, and R. M. Turian, "A New Model for Granular Porous Media: Part I. Model Formulation," *AIChE J.*, **19**, 58 (1973).
Payatakes, A. C., R. Rajagopalan, and C. Tien, "Application of Porous Media Models to the Study of Deep Bed Filtration," *Can. J. Chem. Eng.*, **52**, 727 (1974a).
Payatakes, A. C., C. Tien, and R. M. Turian, "Trajectory Calculation of Particle Deposition in Deep Bed Filtration: Part I. Model Formulation," *AIChE J.*, **20**, 889 (1974b).
Payatakes, A. C., D. H. Brown, and C. Tien, "On the Transient Behavior of Deep Bed Filtration," AIChE Meeting, Houston (1977).
Payatakes, A. C., H. Y. Park, and J. Petrie, "A Visual Study of Particle Deposition and Reentrainment During Depth Filtration of Hydrosols with Polyelectrolyte," *Chem. Eng. Sci.*, **36**, 1319 (1981).
Pendse, H., and C. Tien, "General Correlation of the Initial Collection Efficiency of Granular Filter Beds," *AIChE J.*, **28**, 677 (1982).
Rajagopalan, R., and C. Tien, "Trajectory Analysis of Deep-Bed Filtration Using the Sphere-in-cell Porous Media Model," *AIChE J.*, **22**, 523 (1976).
Rajagopalan, R., and C. Tien, "Single Collector Analysis of Collector Mechanisms in Water Filtration," *Can. J. Chem. Eng.*, **55**, 246 (1977).
Rege, S. D., and H. S. Fogler, "Network Model for Straining Dominated Particle Entrapment in Porous Media," *Chem. Eng. Sci.*, **42**, 1553 (1987).
Rege, S. D., and H. S. Fogler, "A Network Model for Deep Bed Filtration of Solid Particles and Emulsion Drops," *AIChE J.*, **34**, 1761 (1988).
Sahimi, M., G. R. Gavalas, and T. T. Tsotsis, "Statistical and Continuum Models of Fluid-Solid Reactions in Porous Media," *Chem. Eng. Sci.*, **45**, 1453 (1990).
Sharma, M. M., and Y. C. Yortsos, "Transport of Particulate Suspensions in Porous Media: Model Formulation," *AIChE J.*, **33**, 1636 (1987a).
Sharma, M. M., and Y. C. Yortsos, "A Network Model for Deep Bed Filtration," *AIChE J.*, **33**, 1644 (1987b).
Sharma, M. M., and Y. C. Yortsos, "Fines Migration in Porous Media," *AIChE J.*, **33**, 1654 (1987c).
Soo, H., and C. J. Radke, "A Filtration Model for the Flow of Dilute Stable Emulsions in Porous Media: I. Theory," *Chem. Eng. Sci.*, **41**, 263 (1986).
Spielman, L. A., and P. M. Cukor, "Deposition of Non-Brownian Particles Under Colloidal Forces," *J. Colloid Interf. Sci.*, **43**, 51 (1973).
Spielman, L. A., and J. A. FitzPatrick, "Theory for Particle Collection Under London and Gravity Forces," *J. Colloid Interf. Sci.*, **42**, 607 (1973).
Spielman, L. A., and S. L. Goren, "Capture of Small Particles by London Forces from Low-Speed Liquid Flows," *Environ. Sci. Technol.*, **4**, 135 (1970).
Tien, C., and A. C. Payatakes, "Advances in Deep Bed Filtration," *AIChE J.*, **25**, 737 (1979).
Tien, C., *Granular Filtration of Aerosols and Hydrosols*, Ser. in Chem. Eng., Butterworths, Boston (1989).
Tilton, J. N., and A. C. Payatakes, "Collocation Solution of Creeping Newtonian Flow Through Sinusoidal Tubes: a Correction," *AIChE J.*, **30**, 1016 (1984).
Todd, A. C., J. E. Somerville, and G. Scott, "The Application of Depth of Formation Damage Measurements in Predicting Water Injecting Decline," SPE 12498, Denver (1984).
Vaidyanathan, R., and C. Tien, "Hydrosols Deposition in Granular Beds," *Chem. Eng. Sci.*, **43**, 289 (1988).
Wegelin, M., M. Boller, and R. Schertenleib, "Particle Removal by Horizontal-Flow Roughing Filtration," *J. Water SRT—Aqua*, **2**, 80 (1987).
Wegelin, M., R. Schertenleib, and M. Boller, "The Decade of Roughing Filters—Development of a Rural Water-Treatment Process for Developing Countries," *J. Water SRT—Aqua*, **40**, 304 (1991).
Yao, K.-M., M. T. Habidian, and C. R. O'Melia, "Water and Waste Water Filtration: Concepts and Applications," *Environ. Sci. Technol*, **5**, 1105 (1971).

Manuscript received Nov. 9, 1993, and revision received Jan. 27, 1994.